Direct computation of the noise generated by a hot coaxial jet

Christophe Bogey[*], **Sébastien Barré**[†] and **Christophe Bailly**[‡]

Laboratoire de Mécanique des Fluides et d'Acoustique

UMR CNRS 5509, Ecole Centrale de Lyon

69134 Ecully, France

A coaxial jet originating from parallel coplanar pipe nozzles is computed by a compressible Large Eddy Simulation (LES) of 1,800 CPU hours on a Nec SX5, using low-dissipation and low-dispersion numerical schemes in order to determine its generated noise. The jet streams are at high velocities, the primary stream is heated, and the Reynolds number based on the primary velocity and the secondary diameter is around 10^6. High levels of turbulence intensity are also specified at the nozzle exit. The jet aerodynamic development and the near pressure field obtained directly by the LES are presented. The far-field noise is calculated by solving the linear acoustic equations, from the unsteady LES data on cylindrical surfaces surrounding the jet. A good agreement is observed with corresponding noise measurements carried out during the EU CoJeN project in terms of directivity, levels and narrow-band spectra. Some unexpected peaks are however noticed in the simulation spectra, and they are attributed to the development of a Von Karman alley within the inner mixing layer.

I. Introduction

Jet noise simulations developed actively during the last decade, with the aim of providing a better understanding of sound generation, notably by complementing current experimental and theoretical findings,[1,2] as well as reliable predictions for practical flows. The rapid advances in this area have been summarized by Colonius & Lele[3] and by Wang *at al.*[4] The feasibility of computing jet noise directly by solving the unsteady compressible Navier-Stokes equations has been demonstrated for simple configurations. Subsonic single unheated jets at low and moderate Reynolds numbers have thus been calculated by Direct Numerical Simulations and Large Eddy Simulations, by Freund[5] and Bogey *et al.*[6] for instance. These preliminary simulations also allowed us to investigate noise generation mechanisms under controlled conditions. Recent works of the present authors[7,8] were in particular focused on the properties of the two components in subsonic jet noise as the jet Mach and Reynolds numbers vary, and on the correlations between jet turbulence and radiated pressure field.

In order to get closer to realistic jets, there is a need for simulations of more complex configurations, which may be characterized by high Reynolds numbers, high temperatures and coaxial geometries, among other parameters. With this aim in view, the effects of the presence of the nozzle lips in the computational domain have for instance been studied for subsonic jets at high Reynolds numbers by Barré *et al.*[9] and Uzun & Hussaini.[10] Screech noise generation has been studied numerically by Berland *et al.*[11] in a planar underexpanded supersonic jet. Simulations of the sound field obtained from beveled jet nozzles have been also performed by Paliath *et al.*[12] and Viswanathan *et al.*[13] Finally predictions of the noise generated by dual-stream jets have been recently carried out using Large Eddy Simulations by Andersson *et al.*,[14] Vuillemin *et al.*,[15] Mihăescu *et al.*,[16] Viswanathan *et al.*[13] and Tristanto *et al.*[17]

[*]CNRS Research Scientist, christophe.bogey@ec-lyon.fr

[†]PhD., sebastien.barre@dassault-aviation.com, current address: Dassault Aviation, 78 quai Marcel Dassault, Cedex 300, 92552 Saint Cloud Cedex, France

[‡]Professor at Ecole Centrale de Lyon, Senior Member AIAA, christophe.bailly@ec-lyon.fr

Dual-stream nozzles are of interest for the aerospace industry. However, knowledge of aerodynamic development and noise generation in these flow configurations still requires extensive research efforts. Several parameters such as the stream temperatures, the nozzle geometry, the velocity ratio and the inflow conditions are indeed expected to have significant effects on physical mechanisms taking place within these jets. The primary stream of coaxial jets is for instance usually strongly heated, which might affect noise generation according to the controversial debate about the presence of additional dipolar sound sources in hot jets, which is mentioned in Tanna[18] and Viswanathan.[19] Coaxial jets also exhibit complicated flow structures, depending on the mean-velocity ratio between the two streams.[20,21] Measurements of Ko & Kwan[20] within the initial region of coaxial jets isolated for example three mixing regions, which are as many noise generation regions. These authors then proposed to consider coaxial jets as combinations of several single jets, which was later used by Fisher *et al.*[22,23] to formulate basic noise models.

In the present work, a coaxial jet is computed by a compressible Large Eddy Simulation (LES) using low-dissipation and low-dispersion schemes.[24] The near pressure field is determined directly by LES, and extrapolated in far field by solving the linear acoustic equations using LES data recorded on cylindrical surfaces surrounding the jet. The nozzle consists, for simplicity, of parallel pipes, and the nozzle lips are coplanar. The jet streams are at conditions specified in the EU CoJeN project by Mead.[26] The primary and secondary streams are defined by velocities $U_p = 404.5$ m/s and $U_s = 306.8$ m/s, and by static temperatures $T_p = 775.6$ K and $T_s = 288.1$ K. The ratio between the nozzle diameters is $D_s/D_p = 2$. The secondary diameter of the computed jet is $D_s = 4.9$ cm, which leads to the Reynolds number $Re = U_p D_s/\nu = 1.3\times10^6$. For LES concerns, this value is slightly lower than the Reynolds number of the corresponding jet considered in CoJeN experiments. The objectives of the present study are to compute the turbulent development and the pressure field of the coaxial jet by LES, and to assess the accuracy of direct noise prediction for this complex flow configuration, in terms of directivity, levels and narrow-band spectra. The features of the far acoustic field obtained will be therefore compared with CoJeN measurements.[27]

This paper is organized as follows. The parameters of the Large Eddy Simulation of the coaxial jet and those of the extrapolation of the LES near field in the acoustic far field, including in both cases numerical algorithm, computational grids and times, are documented in section II. The jet initial conditions at the exit of the coplanar nozzles are also presented in that section. The main aerodynamic results obtained for the jet are reported in section III. Acoustic near-field and far-field results are then shown and discussed in section IV. To evaluate the accuracy of noise prediction, they are compared with CoJeN data when possible. Concluding remarks are provided in section V.

II. Computational parameters

A. Compressible Large Eddy Simulation of the jet

The LES is performed using an in-house finite-difference solver of the three-dimensional cylindrical filtered compressible Navier-Stokes equations, developed for noise computations using centered[24] and non-centered[25] schemes with low-dissipation and low-dispersion properties. The axis singularity is taken into account by the method of Constantinescu and Lele[28] based on series expansions. Fourth-order eleven-point finite differences are used for spatial discretization, and a second-order six-stage low-storage Runge-Kutta algorithm is applied for time integration. To ensure numerical stability, grid-to-grid oscillations are removed every time step by an explicit eleven-point filtering of the flow variables, which is optimized in the wave-number space to damp only the short waves discretized by fewer than four points per wavelength. The filtering enables also to take into account the effects of the subgrid energy-dissipating scales without affecting significantly the resolved scales, as described in detail in previous works.[29] This LES approach was developed to preserve the Reynolds number given by the inflow conditions, which might not be possible using eddy-viscosity subgrid models such as the dynamical Smagorinsky model.[30,31] Finally, in order to compute the radiated noise directly, non-reflective boundary conditions are implemented, with the addition of a sponge zone in the jet at the outflow.[32]

The LES is conducted on a computational domain of 14 millions of points including two straight pipe nozzles with coplanar lips, which is presented in figure 1. Two overlapping cylindrical grids are used. The first grid of $n_r \times n_\theta \times n_z = 98 \times 48 \times 391$ points is devoted to the interior of the pipes, from $z = -3.3D_s$ to $z = 0$. The second grid of $n_r \times n_\theta \times n_z = 295 \times 48 \times 867$ points contains the jet flow and the acoustic near field. It extends up to $z = 18D_s$ in the axial direction, and to $r = 8D_s$ in the radial direction from the jet axis. In the axial direction, the grid spacing is $0.008D_s$ in the pipe, and up to $z = 1.3D_s$ outside

the nozzle. A stretching rate of 2% is then applied, so that the axial grid spacing is $0.024D_s$ for $z > 2D_s$. The grid is then uniform up to $z = 15D_s$, from which an 8% stretching is used to form the sponge zone. In the radial direction, the mesh spacing is minimum and equal to $0.0045D_s$ at the nozzle walls. It increases outside of the jet flow at a rate of 3.5% to reach $0.052D_s$ for $r > 1.9D_s$ from the jet axis. The sound field is therefore expected to be properly resolved up to Strouhal number $St_{max} = c_{amb}D_s/(U_p \times 4 \times 0.052D_s) = 4$ ($c_{amb} = 340.3$ m/s is the sound speed in the ambient medium, the pressure in the ambient medium is $p_{amb} = 101,325$ Pa).

The LES is performed during 400,000 time steps ($\Delta t_{LES} = 7.4 \times 10^{-8}$ s, or $\Delta t_{LES}U_p/D_s = 6.1 \times 10^{-4}$), and requires an amount of 1,800 CPU hours on a supercomputer Nec SX5. The length of the initial run, before initiating averaging, is 120,000 time steps. The statistics of the flow are therefore calculated during 280,000 time steps, which corresponds to the non-dimensional averaging time of $TU_p//D_s = 170.7$. Time signals of velocity are also recorded in the jet over cylindrical surfaces located at $r = 0$, $D_s/4$, $3D_s/8$ and $D_s/2$ from the centreline, every $50\Delta t_{LES}$ during the final 260,000 LES iterations. For the computation of velocity spectra, they are divided into 25 overlapping sections of length $20,000\Delta t_{LES}$, windowed by a Hanning function.

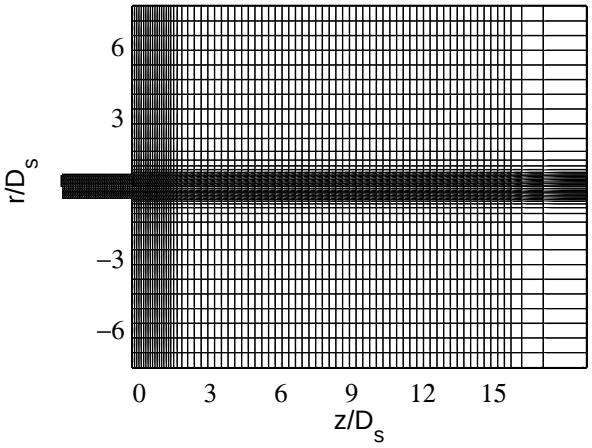

Figure 1. Representation of the (r, z) section of the LES mesh grid. Every 12th grid point is shown in both axial and radial directions.

B. Jet initial parameters

In order to define turbulence conditions at the nozzle exit as realistic as possible at the high Reynolds number of the present Large Eddy Simulation, small velocity disturbances random both in space and in time are added at the pipe inflow to seed the turbulence, in the same way as recently carried out by Barré *et al.*[9] for single-stream jets. The inflow perturbations are growing along the pipes to provide significant turbulence intensities at the nozzle exit. To illustrate the initial conditions thus obtained, the radial profiles of the mean axial velocity and of the RMS levels of the fluctuating axial velocity at the nozzle exit are presented in figure 2. The nozzle-exit boundary layers exhibit thicknesses around $\delta = 0.032D_s$, and peak levels of axial turbulence intensity $u'_{rms}/U_p \simeq 0.14$, 0.08 and 0.12, respectively, from the inner to the outer boundary layers.

When the present method is used in the LES for specifying the jet initial conditions at the nozzle exit, no forcing is applied directly within the jet flow. Previous jet simulations[33] performed without nozzle in the computational domain demonstrated indeed that an intrusive forcing might have a strong influence on jet development and acoustic radiation. Moreover, using this approach, high levels of turbulence intensities can be obtained without generating significant spurious noise. This may enable to avoid the generation of an additional vortex-pairing noise which was likely observed in initially laminar jet flows.[9,34,35] It must be however noted that, because of the numerical cost of the simulation and of the high Reynolds number of the jet, the boundary layers inside the pipe nozzles are under-resolved, which could lead to possible discrepancies with respect to the experiments.

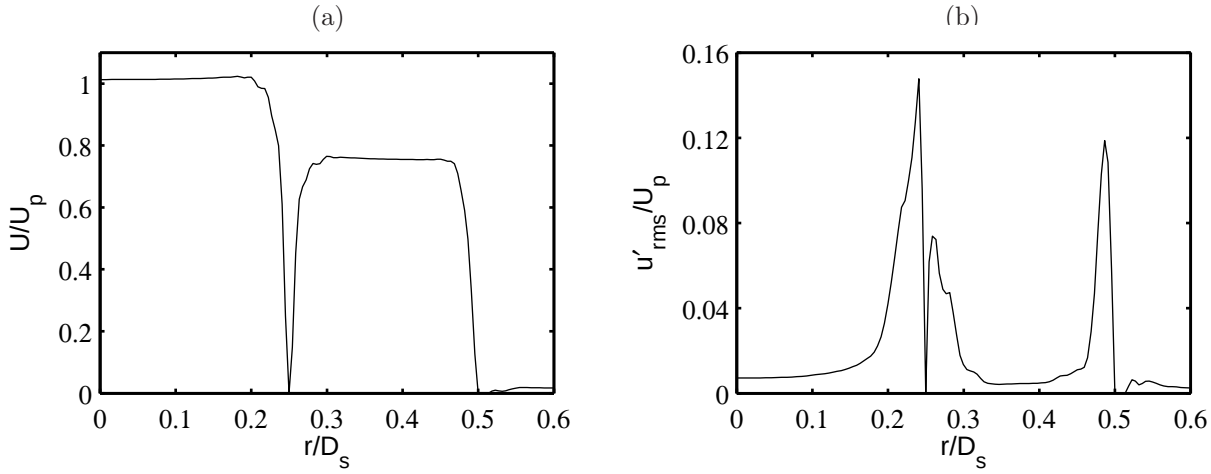

Figure 2. Radial profiles at the exit of the coplanar nozzle at $z = 0$: (a) mean axial velocity, U/U_p; (b) RMS levels of the fluctuating axial velocity, u'_{rms}/U_p.

C. Extrapolation of the LES acoustic field

For the characterization of the noise generated by the coaxial jet, and for the comparison with CoJeN experimental data, the acoustic near field obtained directly by LES is propagated in far field. Different extrapolation methods can be used, such as the Kirchhoff method, see for example the review of Lyrintzis[36] and illustrations in Gloerfelt *et al.*[37] In the present work, the sound propagation is taken into account by solving the linear acoustic equations written for the unknown variables (u', v', w', p'), as in Berland *et al.*,[11] for a cylindrical geometry. The numerical methods used for this calculation are the same as those used for the Large Eddy Simulation, that are optimized eleven-point schemes, and a six-stage Runge Kutta algorithm,[24,25] displaying low dispersion and low dissipation, and non-reflecting conditions[32] at the outflow and outer-side boundaries. The non-centered eleven-point finite differences and filters developed by Berland *et al.*[25] are in particular applied at the inner-side boundaries where the LES data are introduced.

In practice, the LES velocity and pressure are recorded over open cylindrical control surfaces located around the jet at $r = 2D_s$, $3D_s$ and $4D_s$ from the jet axis (hereafter referred to as surfaces S_2, S_3 and S_4), at every point between $0.3D_s \leq z \leq 13.8D_s$, every $25\Delta t_{LES}$ during the final 260,000 LES time steps. The velocity and pressure fluctuations are introduced at the bottom boundary of the cylindrical grid of $n_r \times n_\theta \times n_z = 1201 \times 48 \times 1771$ points (102 millions of points) on which the linear acoustic equations are solved. From the three control surfaces, the noise is propagated at a distance of $60D_s$ from the nozzle exit as in CoJeN experiments,[27] each calculation requiring 80 CPU hours using a Nec SX5. The extrapolation grid used, for instance, when the control surface is surface S_2 at $r = 2D_s$, is presented in figure 3.

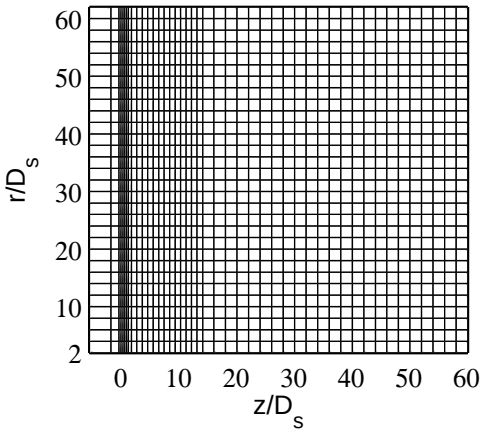

Figure 3. Representation of the (r, z) section of the mesh grid used for the far-field propagation when the control surface is surface S_2 at $r = 2D_s$. Every 40th grid point is shown in both axial and radial directions.

In the axial direction, the discretization is that of the LES for $0 \leq z \leq 14D_s$. A stretching rate of 4% is then applied to get mesh spacings of $0.05D_s$ and $0.1D_s$ in the downstream and upstream directions respectively. In the radial direction, the grid is uniform with a mesh spacing of $0.05D_s$. Therefore the sound field should be accurately calculated up to Strouhal number $St_{max} = c_{amb}D_s/(U_p \times 4 \times 0.05D_s) = 4.2$, which is very similar to the $St_{max} = 4$ obtained in the LES. The time step of the propagation computation, or acoustic time step, is $25\Delta t_{LES}$. As a result, there is no spatial nor temporal interpolation of the LES near-field data. The extrapolation is performed during 14,400 acoustic time steps. In order to study the radiated sound field, pressure signals are recorded around the jet at distances of $40D_s$ and $60D_s$ from the nozzle exit, as it will be illustrated later in figure 13, during 9,200 acoustic time steps (or 230,000 LES time steps, or a non-dimensional time $TU_p//D_s = 140.2$). For the computation of pressure spectra, they are divided into 20 overlapping sections of length corresponding to 876 acoustic time steps, windowed by a Hanning function. The sound spectra are also averaged in the azimuthal direction, over the 48 (r, z) sections of the computational grid.

III. Aerodynamic results

The main aerodynamic results obtained for the coaxial jet by Large Eddy Simulation are reported. Some comparisons with CoJeN preliminary PIV experimental data[38,39] are also shown.

A. Instantaneous flow fields

Snapshots of the vorticity norm and of the static temperature downstream of the nozzle, for $z < 8D_s$, are represented in figure 4. The development of the turbulence, and the mixing of the cold and hot streams within the inner shear layers are clearly visible. The jet growth takes predominantly place in the outer shear layer, whereas a Von Kármán vortex street seems to be observed in the inner shear layer. This behaviour is probably due to the relatively small difference in velocity between the two streams, and it will be discussed later in section III.D. The inner and outer shear layers are moreover found to interact around $z = 2D_s$, before the end of the primary potential core which can be evaluated around $z = 4D_s$. Downstream, the flow appears to be turbulent, even if large spots of high temperature can still be noticed as it is the case in figure 4(b) at $z \simeq 5.5D_s$.

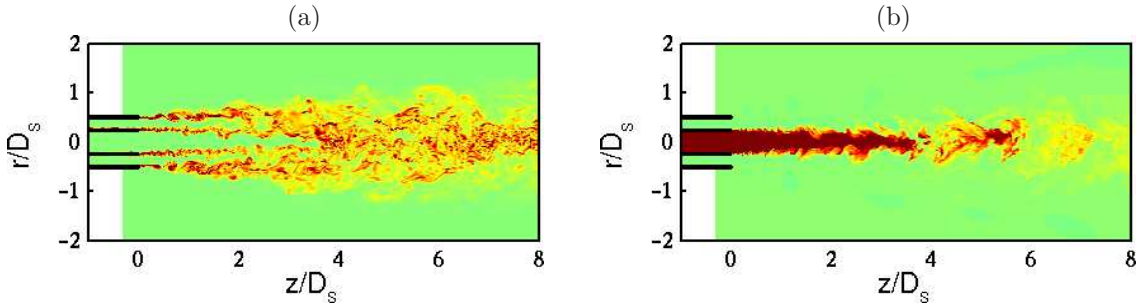

Figure 4. Snapshots in the (r, z) section: (a) vorticity norm $|\omega|$, (b) static temperature T. The color scales are $|\omega| \times D_s/U_p = [0, 12.1]$ and $T = [T_{amb}, T_p]$ respectively.

B. Mean flow fields

In order to characterize the properties of the jet flow, the mean fields of axial and radial velocities, of normal and Reynolds shear stresses, and of turbulent kinetic energy have been computed from the LES data. The field of mean axial velocity U/U_p is for instance shown in figure 5(a). As mentioned above, the primary potential core is longer than the secondary core. The length of the primary core, indicated by $U = 0.95U_p$ on the jet centreline, is more precisely $z_c = 3.5D_s$. The field of mean radial velocity V/U_p is represented in figure 5(b). As it is observed in single jets, the radial velocity exhibits low values of about 3% of the primary velocity. It is also negative outside the jet, which suggests that the entrainment of the surrounding fluid into the jet flow is well taken into account by the boundary conditions of the LES.

As usually in LES, the potential core of the simulated jet is shorter than that estimated in experiments. For the present coaxial jet, $z_c = 5.4D_s$ is for example obtained by CoJeN partners[38,39] using PIV mea-

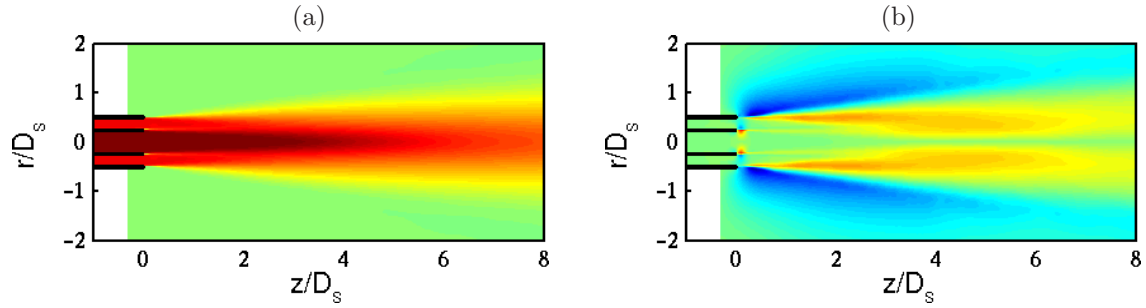

Figure 5. Representation in the (r, z) section: (a) mean axial velocity U, (b) mean radial velocity V. The color scales are $U/U_p = [0, 1]$ and $V/U_p = [-0.03, 0.03]$ respectively.

surements. This discrepancy is often associated with differences in the initial development of the mixing layers. In particular the incoming boundary layers prescribed in simulations are in general thicker than in experiments.[40] Despite this disagreement, the velocity decay along the jet axis is investigated by plotting in figure 6(a) the LES centreline profile of mean velocity U/U_p, as well as the corresponding CoJeN PIV profiles shifted by $-2D_s$ in the axial direction for the comparison. The numerical and experimental velocity decays are found to be very similar. As a final illustration of the LES mean flow, the centreline profile of mean temperature is shown in figure 6(b). The evolution towards the ambient temperature $T_{amb}/T_p = 0.37$ appears quite rapid downstream of the jet core. Unfortunately no experimental data is available for the comparison.

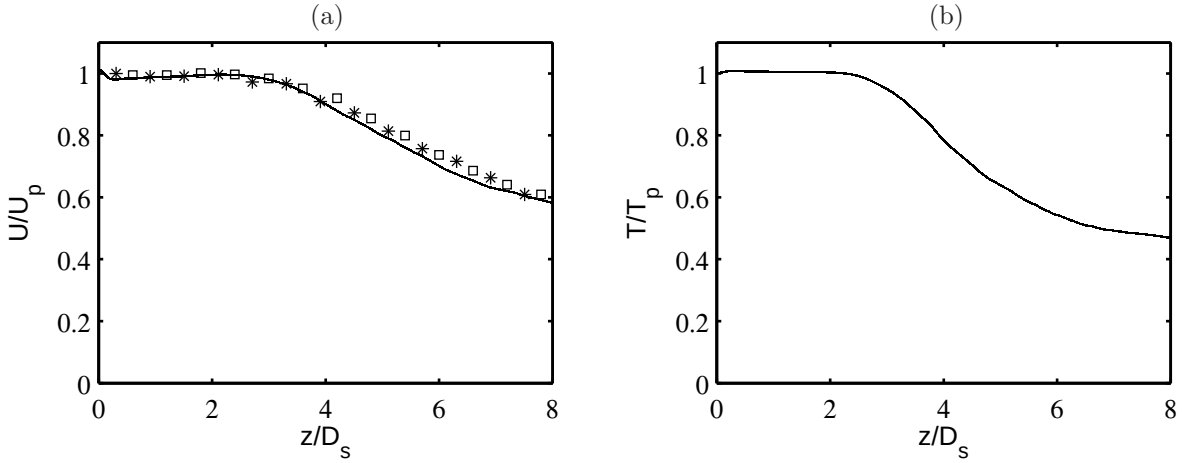

Figure 6. Profiles along the jet centreline, at $r = 0$, of: (a) mean axial velocity, U/U_p; (b) mean temperature, T/T_p. CoJeN PIV measurements made by: □ Universidad Carlos III de Madrid,[38] ∗ University of Warwick,[39] shifted by $-2D_s$ in the axial direction for the comparison.

C. Turbulent flow fields

The RMS levels of the fluctuating axial and radial velocities are presented respectively in figures 7(a) and 7(b). For both components, the higher levels, *i.e.* $u'_{rms} \simeq 0.15U_p$ and $v'_{rms} \simeq 0.12U_p$, are found in the early stage of the outer shear layer, whereas low levels are observed in the inner mixing layer between the two jet streams. Another regions exhibiting significant values of RMS levels are also evidenced downstream, and that is particularly the case for u'_{rms} in figure 7(a). For the axial fluctuating velocity, high RMS values are indeed clearly visible in the zones where the inner and the outer mixing layers merge, and on the axis after the end of the jet potential core.

The centreline profiles of u'_{rms} and v'_{rms} are now displayed in figure 8, and are compared with CoJeN preliminary PIV measurements[38,39] shifted by $-2D_s$ in the axial direction as previously in figure 6. The overall agreement between numerical and experimental curves is fair. The peaks are however reached at axial locations closer to the jet core in the LES. The peak levels obtained from the LES, *i.e.* $u'_{rms} \simeq 0.14U_p$

and $v'_{rms} \simeq 0.10U_p$, are also slightly overestimated with respect to the experimental values $u'_{rms} \simeq 0.12U_p$ and $v'_{rms} \simeq 0.08U_p$.

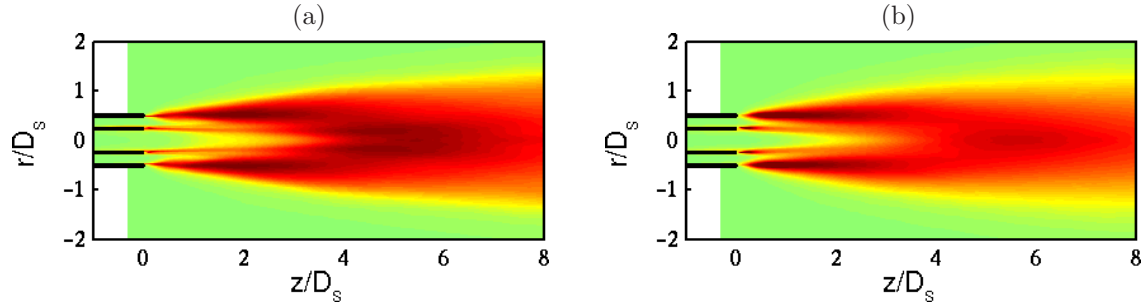

Figure 7. Representation in the (r, z) plane of RMS levels of: (a) the fluctuating axial velocity, u'_{rms}; (b) the fluctuating radial velocity, v'_{rms}. The color scales are $u'_{rms}/U_p = [0, 0.15]$ and $v'_{rms}/U_p = [0, 0.12]$ respectively.

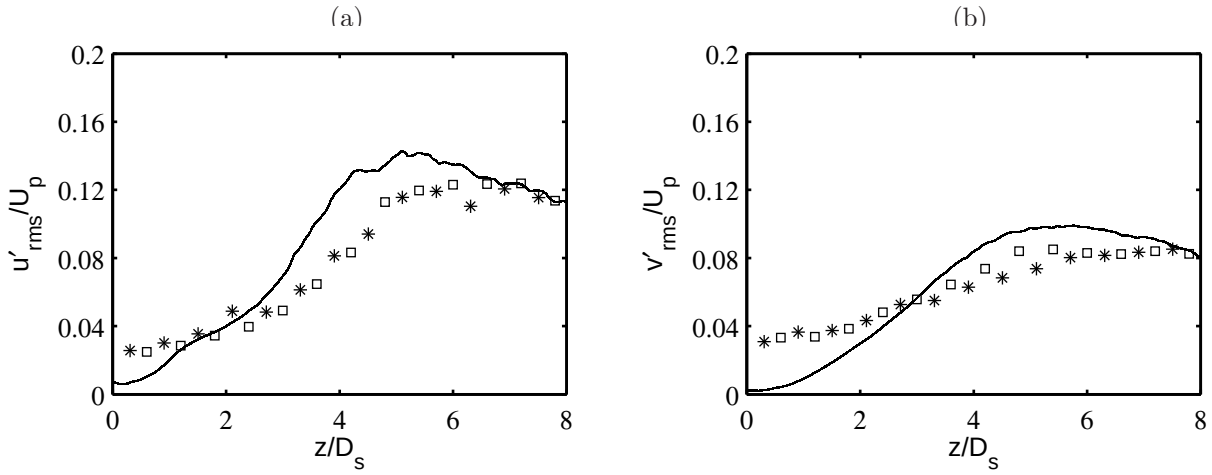

Figure 8. Profiles along the jet centreline, at $r = 0$, of RMS levels of: (a) the fluctuating axial velocity, u'_{rms}/U_p; (b) the fluctuating radial velocity, v'_{rms}/U_p. CoJeN PIV measurements made by: □ Universidad Carlos III de Madrid,[38] ∗ University of Warwick,[39] shifted by $-2D_s$ in the axial direction for the comparison.

D. Turbulence development in the inner mixing layer

Finally the development of the turbulence in the inner mixing layer between the primary hot stream and the secondary cold stream is studied. A snapshot of the azimuthal vorticity field downstream of the inner nozzle lip is shown in figure 9. As mentioned in section III.A, a non-isothermal Von Kármán vortex street is observed, which is in agreement with PIV measurements performed during the CoJeN project.[41] This behaviour should be due to the small difference between velocities U_p and U_s of the primary and secondary streams. This Von Kármán alley also seems to be persistent, and displays several counter-rotating vortex couples as in the CoJeN experiment.

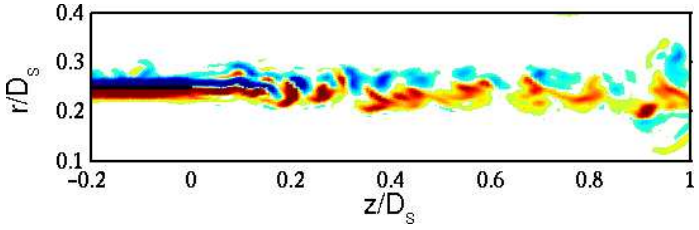

Figure 9. Snapshot in the (r, z) section of the azimuthal vorticity ω_{rz} just downstream of the inner nozzle lip. The color scale is $\omega_{rz} \times D_s/U_p = [-24.3, 24.3]$.

To characterize the Von Kármán alley, velocity spectra have been calculated along the line at $r = D_s/4$

in the inner mixing layer. The spectrum of the fluctuating radial velocity v' obtained at the axial location $z = 0.2D_s$ is presented in figure 10. The spectrum is dominated by peaks with a fundamental peak at Strouhal number $St_{VK} = fD_s/U_p = 8.8$. This peak frequency appears to be the frequency of vortex shedding behind the nozzle lip. Indeed, when the mean velocity and the distance between vortices, calculated from axial correlations of v' velocity, are considered ($U_c = 0.56U_p$ and $\delta_{VK} = 0.064D_s$, respectively, at $z = 0.2D_s$), a Strouhal number $St_{VK} = U_c D_s/(U_p \delta_{VK}) = 8.75$ is obtained.

In the spectrum of figure 10, owing to non-linearity effects, sub-harmonic frequencies are also clearly visible at Strouhal numbers given by $St_{VK} \times i/8$ (i.e. at $St = 1.1$, 2.2, 3.3 etc). Because vortex shedding is an efficient noise generation mechanism, the development of the inner mixing layer in the LES might result in significant contributions to the jet sound field at these frequencies. This possibility is also supported by CoJeN measurements,[41] which show acoustic tones compatible with the vortex street structure observed downstream of the inner nozzle lip.

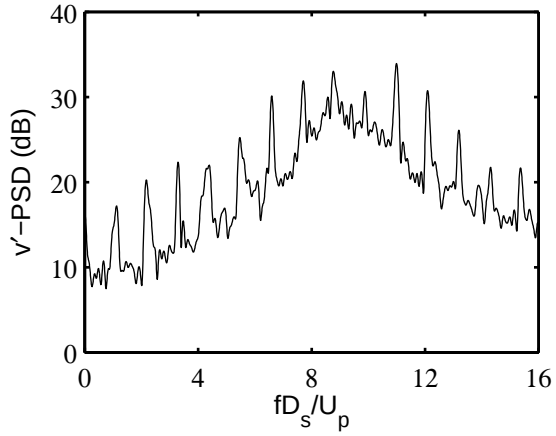

Figure 10. Spectrum of the fluctuating radial velocity v' obtained at $z = 0.2D_s$ and $r = 0.25D_s$, in the inner mixing layer, as a function of Strouhal number fD_s/U_p.

IV. Acoustic results

The near acoustic field determined directly by Large-Eddy Simulation, and the far acoustic field calculated using the extrapolation method are presented in this section. The effects of the numerical procedures on noise prediction are discussed, and comparisons with CoJeN experimental database[27] are shown.

A. Acoustic near field

1. Pressure snapshots

Snapshots of the near pressure field obtained at time step 320,000 for $r \leq 6D_s$ are represented in figure 11. The pressure field provided by Large Eddy Simulation is displayed in figure 11(a), whereas the pressure fields computed by solving the linear acoustical equations using control surfaces S_2, S_3, and S_4, at $r = 2D_s$, $3D_s$, and $4D_s$, are respectively given in figures 11(b), 11(c) and 11(d).

The coupling between the Large Eddy Simulation and the acoustical calculation first seems to occur in an appropriate way. This is suggested by the continuity of the pressure field on either side of the interfaces, indicated by black lines in figures 11(b-d). The near fields determined by extrapolation are very similar. The influence of the choice of the control surface on noise prediction may therefore be weak, which will be investigated quantitatively later. There is also a fair agreement with the near field determined by the LES, even if contributions of aerodynamic pressure[42,43] can be significant in the vicinity of the jet flow in the LES. In addition, the LES pressure field looks to be somewhat dissipated as the radiation distance increases. This might be due to the filtering applied explicitly to the flow variables every LES iteration. The LES time step is indeed very small, with $\Delta t_{LES} c_{amb}/D_s = 5.1 \times 10^{-4}$, which implies that about 2,000 iterations are required for the propagation of acoustic waves over the distance D_s.

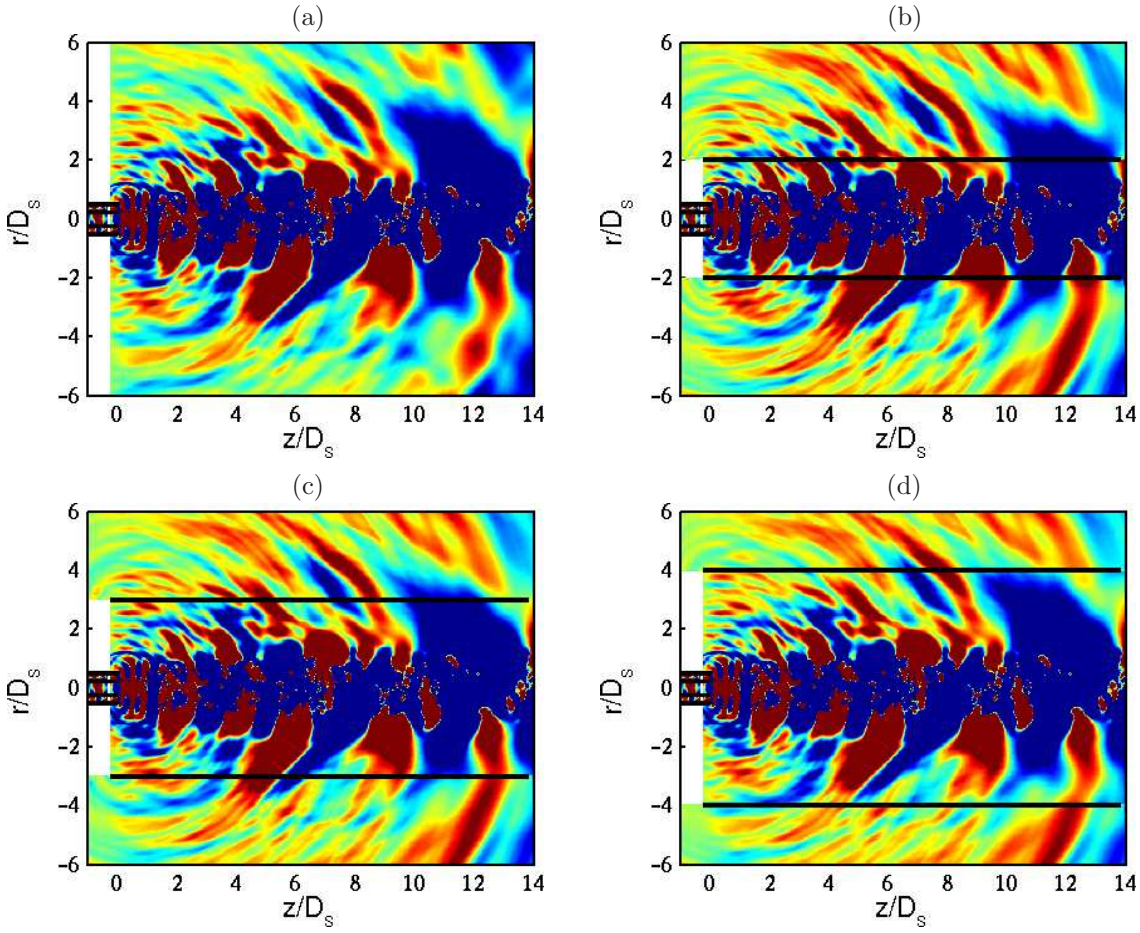

Figure 11. Snapshots of near pressure fields obtained at LES time step 320,000. Representation in the (r, z) section: (a) pressure field calculated directly by LES; (b), (c) and (d) LES pressure field in the central region, and, in peripheral regions, pressure fields computed from the linear acoustic equations using the LES data on the surfaces S_2, S_3 and S_4 located respectively at (b) $r = 2D_s$, (c) $r = 3D_s$, and (d) $r = 4D_s$, indicated by black lines. Color scale is defined for levels between -130 and $+130$ Pa.

2. Near field pressure profiles

Some profiles of near-field pressure are now presented. The profiles obtained along the line located at $r = 2.5D_s$ by LES and by extrapolation using control surface S_2 are first plotted in figure 12(a). A good agreement is observed, despite a constant shift between the two curves. Since the quantity $(p - p_{amb})$ is represented in the LES field, this shift may be associated with a negative contribution of aerodynamic pressure at $r = 2.5D_s$. The present results demonstrate, however, that the extrapolation, and especially the introduction of the LES data at the bottom boundary of the propagation grid, are properly performed.

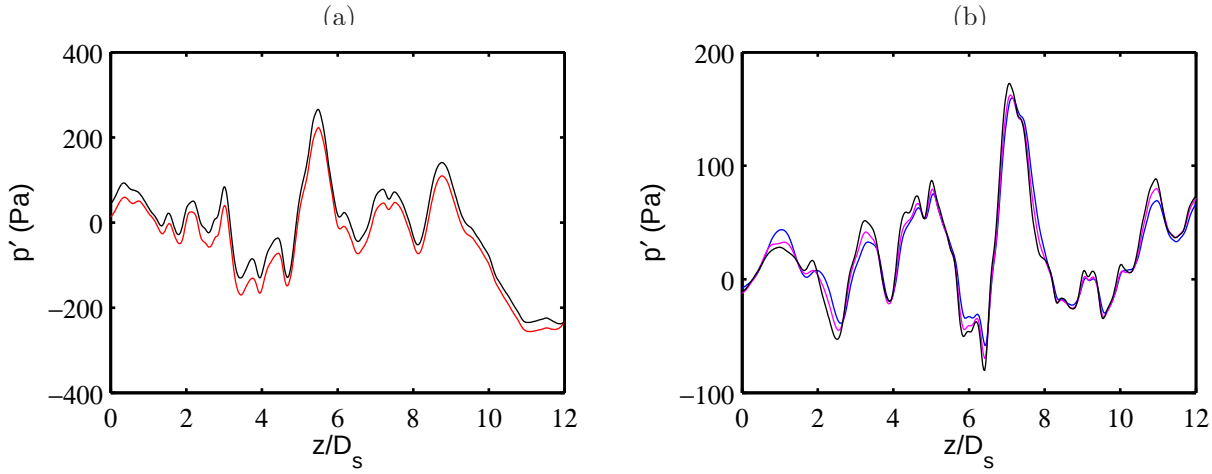

Figure 12. Profiles of the fluctuating pressure obtained at LES time step 320,000 along the lines: (a) at $r = 2.5D_s$, and (b) at $r = 4.5D_s$; ——— from LES, and from the acoustic equations using the control surfaces, ——— S_2 at $r = 2D_s$, ——— S_3 at $r = 3D_s$, ——— S_4 at $r = 4D_s$.

The pressure profiles obtained along the line at $r = 4.5D_s$ by extrapolation of the LES fields at $r = 2D_s$, $3D_s$ and $4D_s$ are shown in figure 12(b). They are quite similar. Thus the sound field computed using the linear acoustical equations does not seem to depend much on the control surface considered. The pressure profiles still seem to be slightly attenuated when the control surface is taken farther from the jet axis. This could be caused by the slight dissipation of the acoustic field that might arise in the LES.

B. Acoustic far-field

1. Pressure snapshots and time signals

A snapshot of the pressure field calculated from the linear acoustic equations is shown in figure 13. The large disparities in length scale between the sound waves and the turbulent region are first clearly illustrated. Some changes in the jet noise features as the emission angle varies are also visible: the acoustic radiation appears to exhibit highest amplitudes and largest wave lengths for angles around 30° relative to the jet direction. A very low-frequency noise is moreover observed, in particular in the sideline and upstream directions. This could unfortunately be parasitic waves generated at the outflow boundary of the LES.

In figure 13, the observation points where pressure signal are recorded are also represented. They are located at $40D_s$ and $60D_s$ from the nozzle exit, for radiation angles between 20° and 90° with respect to the jet direction. As illustrations, the signals obtained at $60D_s$ at radiation angles of 30° and 90° are plotted in figure 14. In a classical way for jet noise,[7,44–46] the noise radiated at 90° appears to contain more high-frequency components, whereas the sideline noise displays a more periodic nature. In figure 14(b), at 90°, a low-frequency component characterized by a non-dimensional period of about $TU_p/D_s = 20$, or by a Strouhal number $St = fD_s/U_p \simeq 0.05$ is also well visible. This component seems to correspond to the spurious noise observed in figure 13. As a result, in what follows, in order not to take into account the non-physical part of the acoustic field, the sound pressure levels are computed only for $St \geq 0.1$.

2. Effects of the propagation

The effects of the far-field extrapolation based on the solving of the acoustical equations are considered. The sound pressure levels obtained at $40D_s$ and $60D_s$ from the nozzle exit using the LES data over control

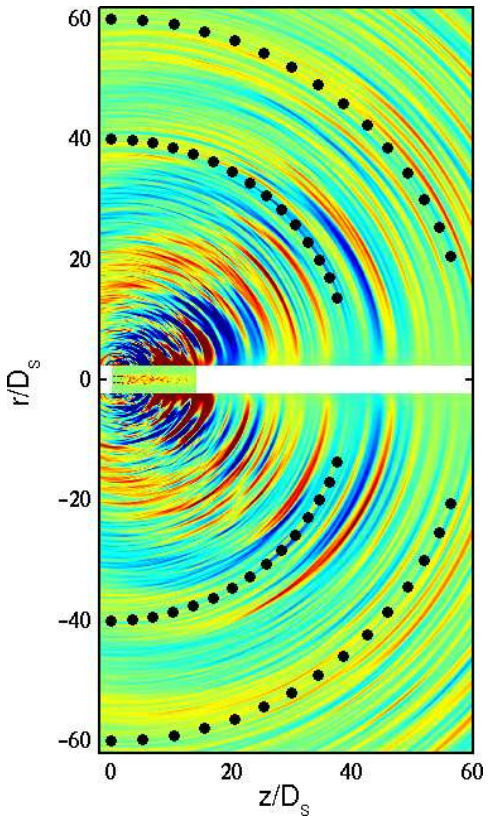

Figure 13. Snapshot of the pressure field obtained at LES time step 320,000 by solving the linear acoustic equations using the control surface S_2, and of the LES vorticity norm in the central region. Color scale is defined for pressure levels between −50 and +50 Pa. The black points indicate the acoustical observation points.

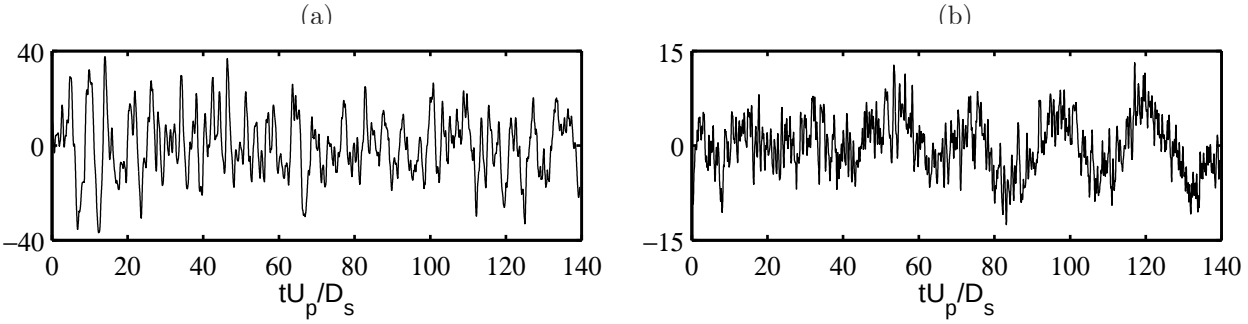

Figure 14. Time signals of the pressure obtained by solving the acoustic equations using the control surface S_2, at $60D_s$ from the nozzle exit and for radiation angles of (a) 30° and (b) 90°, in Pa, as functions of non-dimensional time tU_p/D_s.

surface S_2, and normalized for a distance of $5D_s$ as in CoJeN experiment, are shown in figure 15(a). The results are very close, and even collapse for radiation angles between 40° and 90°, which indicates that the sound propagation is calculated accurately, without significant damping. The maximum difference is lower than 1 dB and is observed for small angles, which may result from the normalization using the nozzle exit as origin whereas the sound sources in the jet are likely to be located farther downstream.

The pressure spectra obtained at 40° from the jet direction using the LES data over control surface S_2 are presented in figure 15(b). Normalized at $5D_s$ from the nozzle exit as previously, the curves computed from the pressure signals at the observation points at $40D_s$ and $60D_s$ compare very well, with a difference by less than 1 dB for Strouhal numbers $St \leq 3$. For higher frequencies, closer to the cut-off Strouhal number $St_{max} = 4.2$ of the filtering estimated in section II.C, a slight attenuation of the acoustic components is nonetheless visible.

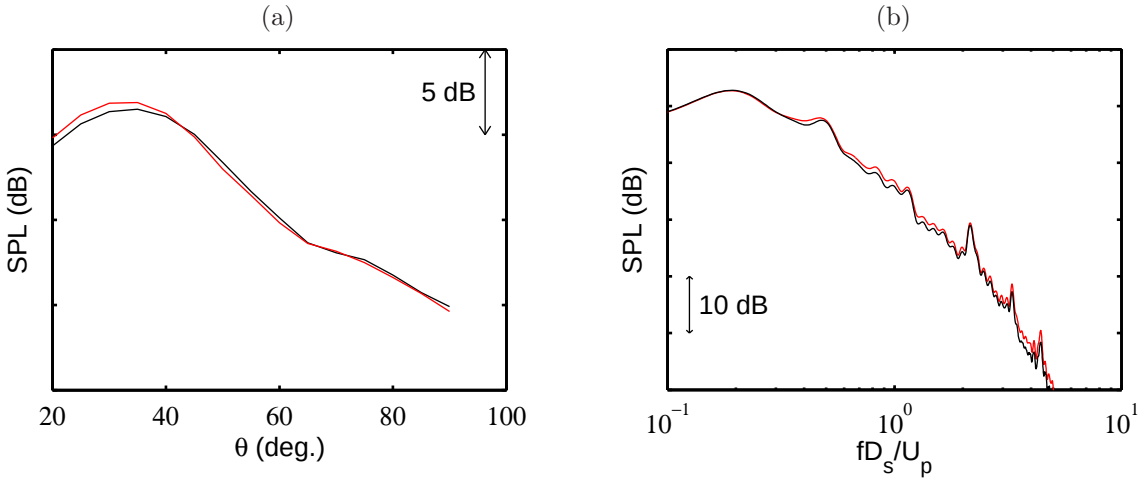

Figure 15. (a) Sound pressure levels calculated for Strouhal numbers $St = fD_s/U_p \geq 0.1$, as a function of the radiation angle relative to the jet direction, and (b) pressure spectra for a radiation angle of 40°, obtained at ——— $40D_s$ and ——— $60D_s$ from the nozzle exit, by solving the acoustical equations using the control surface S_2. The levels are normalized for a propagation distance of $5D_s$.

3. Influence of the control surface

The influence of the control surface on far-field noise prediction is studied. The sound pressure levels obtained at $60D_s$ from the nozzle exit using the LES data over surfaces S_2, S_3 and S_4 are displayed in figure 16. Except for a radiation angle of 50° with respect to the jet direction, the use of a control surface at a larger distance from the centreline leads to a decrease of the sound levels. In the downstream direction, this trend is certainly due to the fact that the control surface is open. Consequently, increasing the distance between the surface and the jet is expected to have the same effects as using a shorter control surface at a fixed location as done for instance in Rahier *et al.*[47] The amount of sound waves emitted by the jet at shallow angles that are not taken into account is more important.

For the noise radiated in the sideline direction, the levels computed from the LES data at $r = 4D_s$ are 1 dB lower than those from the LES data at $r = 2D_s$. The reason for that should not be the open feature of the control surface because the surface, whatever its radial location, encloses most of the sound sources radiating in this direction. However, considering the fact that sideline jet noise usually contains significant high-frequency components, it can be assumed that the present variations of sound levels with the surface location is connected to the possible slight dissipation of the acoustic field in the LES, previously noticed in section IV.A.

In order to characterize the attenuation of the pressure signals when the control surface moves away from the centreline, the pressure spectra obtained for a radiation angle of 40°, at $60D_s$ from the nozzle, are presented in figure 16. The levels computed from the LES data on the three control surfaces S_2, S_3 and S_4 are comparable for low Strouhal numbers $St = fD_s/U_p$, but discrepancies higher than 1 dB appear for $St \geq 0.6$, and they increase with the frequency, the levels at $St = 3$ determined from surfaces S_2 and S_4 differing for instance by 3 dB. For the present simulation, it seems therefore preferable to use the control surface S_2 at $r = 2D_s$, that is the nearest to the jet, in order to minimize the effects of the LES dissipation

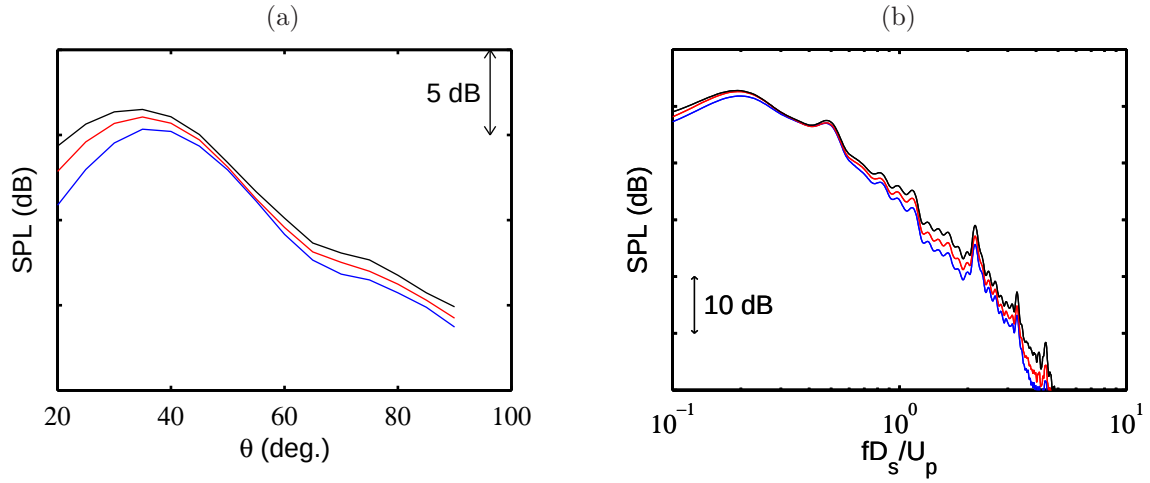

Figure 16. (a) Sound pressure levels calculated for Strouhal numbers $St = fD_s/U_p \geq 0.1$, as a function of the radiation angle relative to the jet direction, and (b) pressure spectra for a radiation angle of 40°, obtained at $60D_s$ from the nozzle exit, by solving the acoustical equations using the control surfaces ——— S_2 at $r = 2D_s$, ——— S_3 at $r = 3D_s$, ——— S_4 at $r = 4D_s$. The levels are normalized for a propagation distance of $5D_s$.

on the sound field. The far-field noise presented in what follows is calculated from that control surface.

4. Azimuthal cross-correlations

The spatial structure of the jet far-field noise is examined by calculating the azimuthal cross-correlations of the fluctuating pressure obtained using control surface S_2, at $60D_s$ from the nozzle exit. The broadband pressure signals are considered for the calculation. The correlation functions obtained at 30° and 60° relative to the jet are shown in figure 17. The correlation levels are very high at the radiation angle of 30°, for which the correlation is even nearly 0.8 for an azimuthal separation angle of 180°. At the emission angle of 60°, the correlation levels are still significant but they are appreciably lower. A similar decrease with the radiation angle is observed in single-stream jets,[7,48,49] and this behaviour has been associated with the jet noise components and sources. The present curves thus provide a first insight into the noise generation in the coaxial jet.

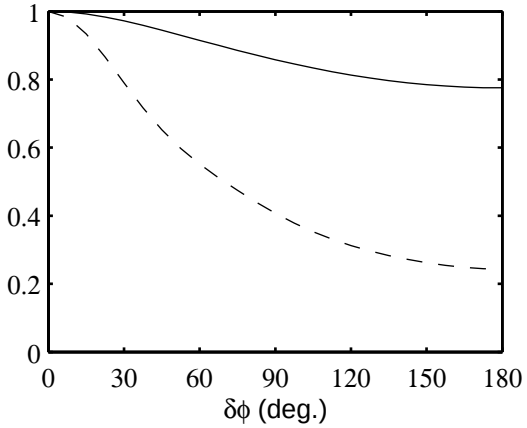

Figure 17. Azimuthal cross-correlation functions of the fluctuating pressure obtained using control surface S_2, at $60D_s$ from the nozzle exit and for radiation angles of: ——— 30°, − − − 60°.

5. Comparison with CoJeN experimental data

The acoustic field computed by Large Eddy Simulation and extrapolated in far field by the linear acoustic equations using control surface S_2 at $r = 2D_s$ is finally compared with CoJeN experimental data.[27]

The numerical and experimental sound pressure levels obtained at $60D_s$ from the nozzle exit and normalized at $5D_s$ are presented in figure 18. The levels are calculated over the Strouhal number range $St = fD_s/U_p \geq 0.1$. The agreement between the simulation and the experiment is very satisfactory, with no more than 3 dB between the results whatever the radiation angle may be. The LES sound levels are however higher at any angle. The overestimation is by 1.5 dB at the predominant radiation angle of 30°, and it increases at larger angles. It can also be noted that the effects of filtering the sound levels for $St \geq 0.1$ are weak. From the experimental data, there are indeed very small differences between the overall sound levels (red mixed line) and the levels filtered for $St \geq 0.1$ (red solid line).

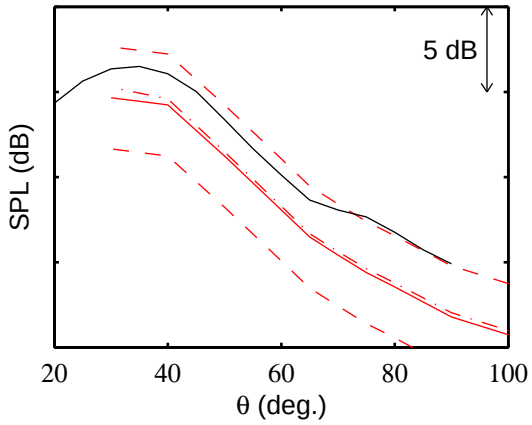

Figure 18. Sound pressure levels obtained at $60D_s$ from the nozzle exit, as a function of the radiation angle relative to the jet direction. Levels calculated for Strouhal numbers $St = fD_s/U_p \geq 0.1$: ——— simulation results using control surface S_2, ——— CoJeN experimental data,[27] – – – experimental data ±3dB. Overall sound pressure levels, calculated for $St \geq 0$: – · – · experimental data. The levels are normalized for a propagation distance of $5D_s$.

The narrow-band sound pressure spectra calculated at the radiation angles of 30°, 40°, 60° and 90° are plotted in figure 19(a-d). Some peaks are visible in the spectra, especially at Strouhal numbers 1.1, 2.2, 3.3 and 4.4. These noise frequencies correspond to the sub-harmonic frequencies that are observed in velocity spectra obtained in the initial stage of the inner mixing layer, as in figure 10. In the same way as it was assumed from CoJeN experimental results,[41] these tones may be generated by the development of the Von Kármán vortex street exhibited in figure 9. They could also be one of the reasons of the overestimation of the sound levels with respect to the measurements.

The numerical spectra agree, however, well with the experimental spectra both in terms of overall shape and levels, from $St = 0.1$ up to a Strouhal number between 2 and 3, the cut-off Strouhal number of the simulation being around $St = 4$. The agreement is clearly illustrated for example in figure 19(b) with the results at 40° from the jet direction. The changes in the sound spectra with the radiation angles are also well predicted by the simulation. The pressure spectra especially broaden as the radiation angle increases, which is similar to what is observed for single-stream jets.[7,44–46] Finally the results likely indicate that the turbulent noise sources in the present coaxial jet at a high Reynolds number are properly taken into account by the LES.

V. Conclusion

This paper presents the Large Eddy Simulation (LES) of a coaxial jet at conditions specified in the EU CoJeN project, which provides also both aerodynamic and acoustic experimental data. With the aim of computing directly practical jet noise, this simulation is a step forward because the flow configuration is much more complex (coaxial geometry, heated primary stream, high Reynolds number) than in our previous studies. The jet considered is also more realistic regarding aeronautic applications.

The simulation is based on low-dissipation and low-dispersion schemes, and unfortunately is computationally very expensive, which might prevent us from performing parametric studies in the short term. Very satisfactory results are however obtained for the acoustic far-field directly obtained by the LES, without resorting to acoustical modelling. Sound pressure spectra and levels compare indeed well with corresponding CoJeN measurements, at any radiation angle. Some discrepancies attributed to numerical or physical

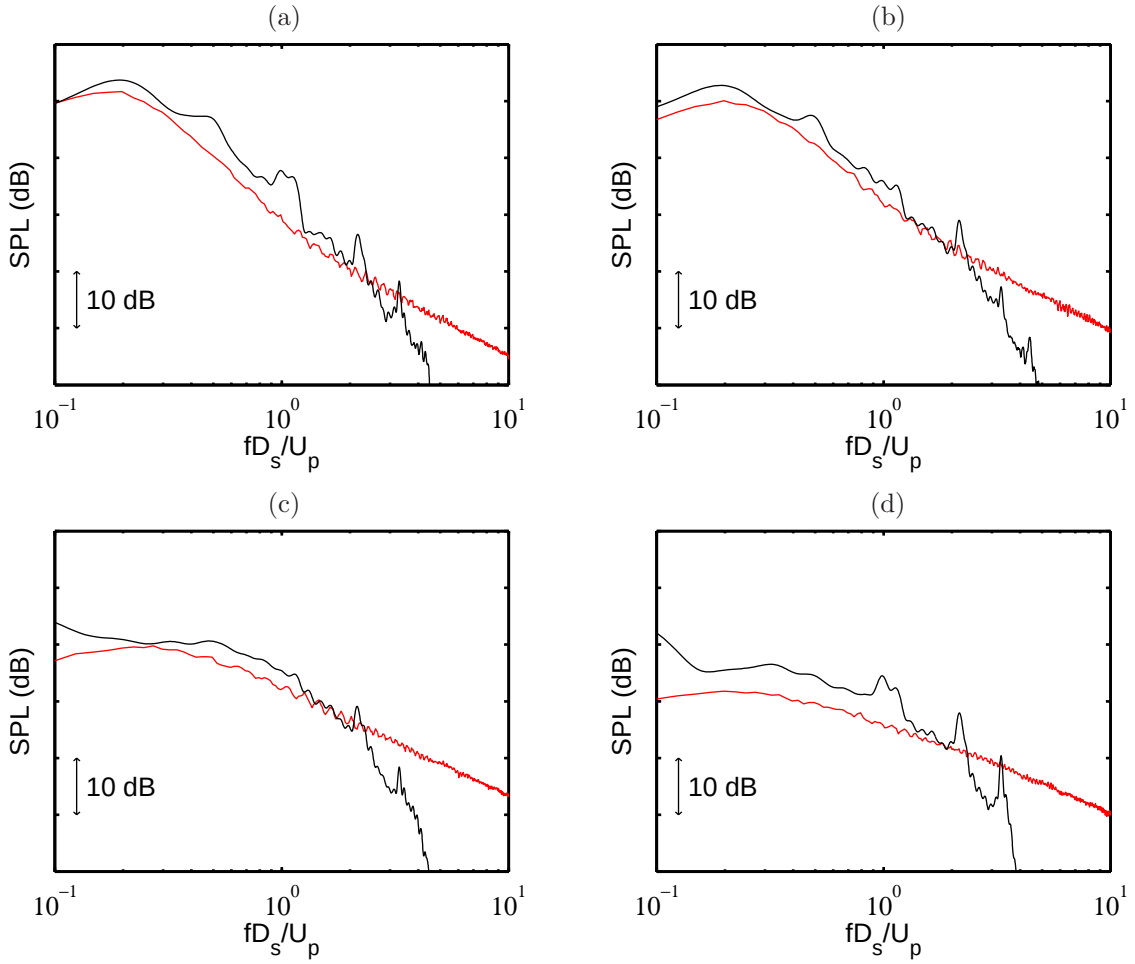

Figure 19. Pressure spectra obtained at $60D_s$ from the nozzle exit: ——— simulation results using the control surface S_2 and ——— CoJeN experimental data,[27] for radiation angles relative to the jet direction of: (a) 30^o, (b) 40^o, (c) 60^o, (d) 90^o, as functions of Strouhal number $St = fD_s/U_p$. The levels are normalized for a propagation distance of $5D_s$.

artefacts have been still noticed. They have been identified in order to improve noise prediction in future simulations.

Finally the simulation generated an unsteady database both for the turbulent flow and for the sound field of the coaxial jet, which could be used in further works for investigating noise generation mechanisms, as it was done for instance for single-stream jets in a previous reference.[8]

Acknowledgments

This work is supported by the EU Sixth Framework Project CoJeN (Computation of Coaxial Jet Noise, EC Contract No. AST3-CT-2003-502790). The authors gratefully acknowledge the Institut du Développement et des Ressources en Informatique Scientifique (IDRIS - CNRS) for providing computing time and for its technical assistance. A part of the computations was also carried out on one of the supercomputers of the CEA (the French Atomic Energy Agency).

References

[1]Tam, C.K.W., "Jet noise: since 1952," *Theoret. Comput. Fluid Dynamics*, Vol. 10, 1998, pp. 393-405.

[2]Tam, C.K.W., "Supersonic jet noise," *Annu. Rev. Fluid Mech.*, Vol. 27, 1995, pp. 17-43.

[3]Colonius, T. and Lele, S.K., "Computational aeroacoustics: progress on nonlinear problems of sound generation," *Progress in Aeroospace Sciences*, Vol. 40, 2004, pp. 345-416.

[4]Wang, M., Freund J.B, and Lele, S.K., "Computational prediction of flow-generated sound," *Annu. Rev. Fluid. Mech.*, Vol. 38, 2006, pp. 483-512.

[5]Freund, J.B., "Noise sources in a low-Reynolds-number turbulent jet at Mach 0.9," *J. Fluid Mech.*, Vol. 438, 2001, pp. 277-305.

[6]Bogey, C., Bailly, C., and Juvé, D., "Noise investigation of a high subsonic, moderate Reynolds number jet using a compressible LES," *Theoret. Comput. Fluid Dynamics*, Vol. 16, No. 4, 2003, pp. 273-297.

[7]Bogey, C. and Bailly, C., "Investigation of downstream and sideline subsonic jet noise using Large Eddy Simulations," *Theoret. Comput. Fluid Dynamics*, Vol. 20, No. 1, 2006, pp. 23-40.

[8]Bogey, C. and Bailly, C., "An analysis of the correlations between the turbulent flow and the sound pressure fields of subsonic jets," *J. Fluid Mech.*, 2007, in press. See also AIAA Paper 2005-2995.

[9]Barré, S., Bogey, C., and Bailly, C., "Computation of the noise radiated by jets with laminar/turbulent nozzle-exit conditions," AIAA Paper 2006-2443, 2006.

[10]Uzun, A. and Hussaini, M., "High frequency noise generation in the near-nozzle region of a jet," AIAA 2006-2499, 2006.

[11]Berland, J., Bogey, C., and Bailly, C., "Numerical study of screech generation in a planar supersonic jet," *Phys. Fluids*, Vol. 19, 2007, in press. See also AIAA Paper 2006-2496.

[12]Paliath, U. and Morris, P.J., "Prediction of jet noise from circular beveled nozzles," AIAA Paper 2005-3096, 2005.

[13]Viswanathan, K., Shur, M.L., Spalart, P.R., and Strelets, M.Kh., "Computation of the flow and noise of round and beveled nozzles," AIAA Paper 2006-2445, 2006.

[14]Andersson, N., Eriksson, L.-E., and Davidson, L., "LES prediction of flow and acoustic field of a coaxial jet," AIAA Paper 2005-2884, 2005.

[15]Vuillemin, A., Loheac, P., Rahier, G., Vuillot, F., and Lupoglazoff, N., "Aeroacoustic numerical method assessment for a double stream nozzle," AIAA Paper 2005-3043, 2005.

[16]Mihăescu, M., Gutmark, E., Szasz, R.-Z., and Fuchs, L., "Flow and acoustics of a coaxial nozzle: a sensitivity to the inlet boundary conditions," AIAA Paper 2006-1387, 2006.

[17]Tristanto, I.H., Page, G.J., and McGuirk, J.J., "Large Eddy Simulation of hot coaxial jets," AIAA Paper 2006-2497, 2006.

[18]Tanna, H.K., "An experimental study of jet noise. Part I: Turbulent mixing noise," *J. Sound Vib.*, Vol. 50, No. 3, pp. 405-428.

[19]Viswanathan, K., "Aeroacoustics of hot jets," *J. Fluid Mech.*, Vol. 516, 2004, pp. 39-82.

[20]Ko, N.W.M. and Kwan, A.S.H, "The initial region of subsonic coaxial jets," *J. Fluid Mech.*, Vol. 73, No. 2, 1976, pp. 305-332.

[21]da Silva, C.B., Balarac, G., and Métais O., "Transition in high velocity ratio coaxial jets analysed from direct numerical simulations," *J. Turbulence*, Vol. 4, 2003, 024.

[22]Fisher, M.J., Preston, G.A., and Mead, C.J., "A modelling of the noise from simple coaxial jets, part I: With unheated primary flows," *J. Sound Vib.*, Vol. 209, No. 3, 1998, pp. 385-403.

[23]Fisher, M.J., Preston, G.A., and Mead, C.J., "A modelling of the noise from simple coaxial jets, part II: With heated primary flows," *J. Sound Vib.*, Vol. 209, No. 3, 1998, pp. 405-417.

[24]Bogey, C. and Bailly, C., "A family of low dispersive and low dissipative explicit schemes for flow and noise computations," *J. Comput. Phys.*, Vol. 194, No. 1, 2004, pp. 194-214.

[25]Berland, J., Bogey, C., Marsden, O., and Bailly, C., "High-order, low dispersive and low dissipative explicit schemes for multiple-scale and boundary problems," *J. Comput. Phys.*, 2007, doi:10.1016/j.jcp.2006.10.017.

[26]Mead, C.J., "Specification of nozzles and flow conditions for CoJeN," CoJeN deliverable 0.1, Sixth Framework Programme, EC Contract No. AST3-CT-2003-502790, 2004.

[27]Mead, C.J., "Acoustic measurements," CoJeN deliverable 3.9, Sixth Framework Programme, EC Contract No. AST3-CT-2003-502790, 2007.

[28]Constantinescu, G.S. and Lele, S.K., "A highly accurate technique for the treatment of flow equations at the polar axis in cylindrical coordinates using series expansions," *J. Comput. Phys.*, Vol. 183, 2002, pp. 165-186.

[29]Bogey, C. and Bailly, C., "Large Eddy Simulations of transitional round jets: influence of the Reynolds number on flow development and energy dissipation," *Phys. Fluids*, Vol. 18, No. 6, 2006, 065101.

[30]Bogey, C. and Bailly, C., "Decrease of the effective Reynolds number with eddy-viscosity subgrid-scale modeling," *AIAA Journal*, Vol. 43, No. 2, 2005, pp. 437-439.

[31]Bogey, C. and Bailly, C., "Large Eddy Simulations of round free jets using explicit filtering with/without dynamic Smagorinsky model," *Int. J. Heat and Fluid Flow*, Vol. 27, No. 4, 2006, 603-610.

[32]Bogey, C. and Bailly, C., "Three-dimensional non reflective boundary conditions for acoustic simulations: far-field formulation and validation test cases," *Acta Acustica*, Vol. 88, No. 4, 2002, pp. 463-471.

[33]Bogey, C. and Bailly, C., "Effects of inflow conditions and forcing on a Mach 0.9 jet and its radiated noise," *AIAA Journal*, Vol. 43, No. 5, 2005, pp. 1000-1007.

[34]Zaman, K.B.M.Q., "Effect of the initial condition on subsonic jet noise," *AIAA Journal*, Vol. 23, No. 9, 1985, pp. 1370-1373.

[35]Bridges, J.E. and Hussain, A.K.M.F., "Roles of initial conditions and vortex pairing in jet noise," *J. Sound Vib.*, Vol. 117, No. 2, 1987, pp. 289-311.

[36]Lyrintzis, A.S., "Surface integral methods in computational aeroacoustics-From the (CFD) near-field to the (Acoustic) far-field," *International Journal of Aeroacoustics*, Vol. 2, No. 2, 2003, pp. 95-128.

[37]Gloerfelt, X., Bailly, C., and Juvé, D., "Direct computation of the noise radiated by a subsonic cavity flow and application of integral methods," *J. Sound Vib.*, Vol. 266, No. 1, 2003, pp. 119-146.

[38]Lecuona, A., Nogueira, J., Rodríguez, P.A., Acosta, A., Alfaro, J.A., Nauri, S., and Legrand, M., "Preliminary notes on the whole field PIV measurements provided by UCM3," CoJeN private communication, 2007.

[39]Skeen, A., "Warwick phase 3 PIV data," CoJeN private communication, 2007.

[40]Zaman, K.B.M.Q., "Far-field noise of a subsonic jet under controlled excitation," *J. Fluid Mech.*, Vol. 152, 1985, pp. 83-111.

[41]Nogueira, J., Legrand, M., Nauri, S., Rodríguez, P.A., and Lecuona, A., "Analysis of the vortex street generated at the core-bypass lip of a jet engine nozzle," *PivNet2 Final Workshop*, Göttingen, Germany, September 7-8, 2006.

[42]Arndt, R.E.A, Long, D.F., and Glauser, M.N., "The proper orthogonal decomposition of pressure fluctuations surrounding a turbulent jet," *J. Fluid Mech.*, Vol. 340, 1997, pp. 1-33.

[43]Coiffet, F., Jordan, P., Delville, J., Gervais, Y., and Ricaud, F., "Coherent structures in subsonic jets: a quasi-irrotational source mechanism?," *International Journal of Aeroacoustics*, Vol. 5, No. 1, 2005, pp. 67-89.

[44]Mollo-Christensen, E., Kolpin, M.A., and Martucelli, J.R., "Experiments on jet flows and jet noise far-field spectra and directivity patterns," *J. Fluid Mech.*, Vol. 18, 1964, pp. 285-301.

[45]Lush, P.A., "Measurements of subsonic jet noise and comparison with theory," *J. Fluid Mech.*, Vol. 46, No. 3, 1971, pp. 477-500.

[46]Ahuja, K.K., "Correlation and prediction of jet noise," *J. Sound Vib.*, Vol. 29, No. 2, 1973, pp. 155-168.

[47]Rahier, G., Prieur, J., Vuillot F., Lupoglazoff, N., and Biancherin A., "Investigation of integral surface formulations for acoustic predictions of hot jets starting from unsteady aerodynamic simulations," AIAA Paper 2003-3164, 2003.

[48]Maestrello, L., "Two points correlations of sound pressure in the far field of a jet: Experiment," NASA-TMX-72835, 1976.

[49]Juvé, D., Sunyach, M., and Comte-Bellot, G., "Filtered azimuthal correlations in the acoustic far field of a subsonic jet," *AIAA Journal*, Vol. 17, No. 1, 1979, pp. 112-113.